

# SOLAR HARD X-RAY BURSTS

BRIAN R. DENNIS

*Laboratory for Astronomy and Solar Physics, NASA Goddard Space Flight Center,  
Greenbelt, MD 20771, U.S.A.*

**Abstract.** The major results from SMM are presented as they relate to our understanding of the energy release and particle transportation processes that lead to the high-energy X-ray aspects of solar flares. Evidence is reviewed for a 152–158 day periodicity in various aspects of solar activity including the rate of occurrence of hard X-ray and gamma-ray flares. The statistical properties of over 7000 hard X-ray flares detected with the Hard X-Ray Burst Spectrometer are presented including the spectrum of peak rates and the distribution of the photon number spectrum. A flare classification scheme introduced by Tanaka is used to divide flares into three different types. Type A flares have purely thermal, compact sources with very steep hard X-ray spectra. Type B flares are impulsive bursts which show double footpoints in hard X-rays, and soft-hard-soft spectral evolution. Type C flares have gradually varying hard X-ray and microwave fluxes from high altitudes and show hardening of the X-ray spectrum through the peak and on the decay. SMM data are presented for examples of type B and type C events. New results are presented showing coincident hard X-rays, O v, and UV continuum observations in type B events with a time resolution of  $\leq 128$  ms. The subsecond variations in the hard X-ray flux during  $\lesssim 10\%$  of the stronger events are discussed and the fastest observed variation in a time of 20 ms is presented. The properties of type C flares are presented as determined primarily from the non-imaged hard X-ray and microwave spectral data. A model based on the association of type C flares and coronal mass ejections is presented to explain many of the characteristics of these gradual flares.

## 1. Introduction

This paper is a review of some of the more recent results on solar hard X-ray bursts primarily for the Solar Maximum Mission (SMM). I have used the flare classification scheme introduced by Tanaka (1983) to lend some order to the apparently random nature of hard X-ray bursts.

It is instructive to first reflect on the state of our knowledge of hard X-ray bursts prior to the immense number of observations during this solar maximum, now determined to have been in December, 1979. Prior to that time there were no hard X-ray images of solar flares apart from observations of over-the-limb events, no observations of variations on time-scales much less than 1 s, no spectral observations that could resolve the steepest spectra, and no definitive polarization measurements at all. We now have X-ray images for many flares with better than  $10''$  resolution at energies up to 30 keV from SMM and 40 keV from Hinotori. The Hard X-Ray Burst Spectrometer (HXRBS) has provided observations of over 7000 flares with a time-resolution of 128 ms and many of these with 10 ms resolution. Significant advances in spectral resolution and in polarization measurements have also been made but only in relatively short duration observations. Lin *et al.* (1981) observed one flare and several microflares with sub-keV resolution on a balloon flight and were able to resolve the X-ray spectrum which became as steep as  $E^{-11}$  at photon energies  $E$  up to 35 keV. Tramiel *et al.* (1984) made

polarization measurements in the energy range from 5 to 20 keV on a flight of the Space Shuttle and obtained upper limits between 2.5 and 12.7% that are consistent with the more sophisticated polarization models of Leach and Petrosian (1983).

What have we learned from the new observations? In this paper I will concentrate on the answers to this question that concern the improvements in our knowledge of the flare processes that lead to the production of hard X-rays. In particular I will show that we have begun to be able to differentiate, in some specific flares, between the three basic models for the production of hard X-rays: thick and thin-target interactions, and thermal (Brown 1971; Lin and Hudson, 1976; Tucker, 1975; Crannell *et al.*, 1978).

Although it is almost universally accepted that the hard X-rays are electron-ion bremsstrahlung, the determination of the spectrum of the emitting electrons still depends on knowledge of the temperature and density of the plasma with which the electrons are interacting. It is necessary to know, in any particular flare, which model (or combination of models) is correct since the determination of the electron spectrum from the observed X-ray spectrum depends on the model assumed. More importantly, the correct model must be known in order to determine the role of the fast electrons in the overall flare energetics, and ultimately to determine the fundamental energy release mechanism or mechanisms of the flare. It now appears clear, as indicated below, that different models apply for different flares and at different times during individual flares.

This paper begins in Section 2 with a discussion of the results which have been obtained from a statistical analysis of the flares detected with HXRBS including evidence for a 158 day periodicity, the spectrum of peak counting rates, and the distribution of spectra. The flare classification scheme is presented in Section 3 and properties of types B and C flares are presented in Sections 4 and 5, respectively.

## 2. Statistical Analysis

One of the first things that can be done with the large number of events recorded with instruments on SMM is to determine the global properties of flares including the rate of occurrence, the spectrum of sizes, rise times, durations, spectral parameters, etc. Several catalogues of SMM events have already been prepared and distributed. These included the SMM Event Listing for 1980 (Pryor *et al.*, 1981) and the HXRBS Events Listing for 1980–82 (Dennis *et al.*, 1983). A comprehensive catalogue of data on all SMM events is available on the VAX computer at the SMM Data Analysis Center and plans exist to issue, in the near future, a revised version of the 1980 listing, a complete listing of all HXRBS events, and a new listing of all SMM events recorded since the repair.

### 2.1. THE 152–158 DAY PERIODICITY

The most notable result from this statistical analysis is the discovery of a 152–158 day periodicity in the rate of flare occurrence during this solar cycle, cycle 21. This periodicity was first noticed by Rieger *et al.* (1985) in the tendency of 139 solar flares detected with the Gamma Ray Spectrometer (GRS) above 300 keV to occur in groups with a mean spacing of 154 days.

A much larger sample of 6775 hard X-ray flares detected with HXRBS above  $\sim 30$  keV was used by Kiplinger *et al.* (1985) to reveal a similar periodicity illustrated in Figure 1. The number of flares detected per day by HXRBS is plotted vs time from launch in 1980 until the middle of 1984 with corrections made for the SMM duty cycle. A power spectrum analysis of the data plotted in Figure 1 was carried out using a Fourier transform routine that allows for the data gaps (Deeming, 1975) and this confirms the existence of a strong Fourier component having a period of 158 days and a semi-amplitude of approximately 40% of the mean flare rate. The sine wave superposed on the data in Figure 1 represents this Fourier component plus the first-order trend. Eight peaks can be seen in the flare rate at the expected times given by the sine wave up to June, 1983. The expected peak in the fall of 1983 was not present but a ninth strong peak was observed in April/May, 1984. Subsequently, no increase in flare rate was observed in the fall of 1984 but some weak activity was observed in January/February, 1985.

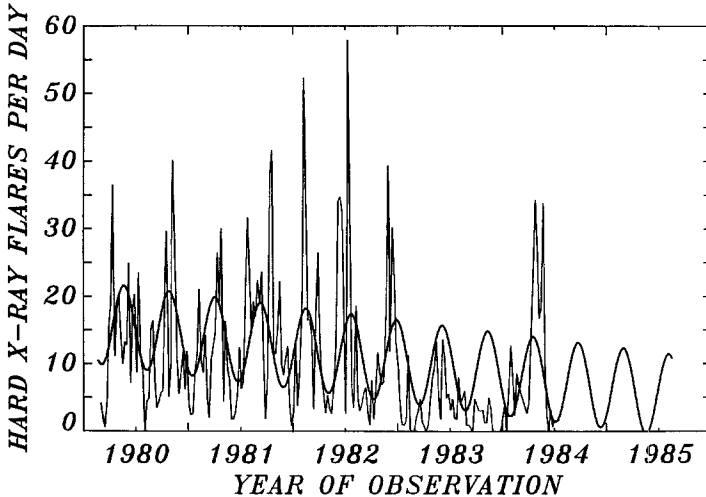


Fig. 1. Plot of the weekly averaged rate of flares detected with HXRBS (corrected for the duty cycle) as a function of time from launch in February 1980 until after the repair in April 1984. The sine wave superimposed on the data is the Fourier component with a period of 158 days determined from the power spectrum analysis. A total of 6675 flares were included in the analysis. The energy threshold varied from 25 keV at launch to 33 keV in 1984.

A similar periodic component is present in an analysis of 6102 events with X-ray emission that does not exceed 150 keV. The power spectrum of this data set shown in Figure 2 also shows a strong peak at  $0.0633 \text{ days}^{-1}$  corresponding to a period of the 139 gamma-ray flares used by Rieger *et al.* (1985). A periodicity of 152 days is also present in the rate of GOES events with a classification above M2.5 (Rieger *et al.*, 1985), and Bogart and Bai (1985) report a 157 day periodicity of flare occurrence in the microwave data.

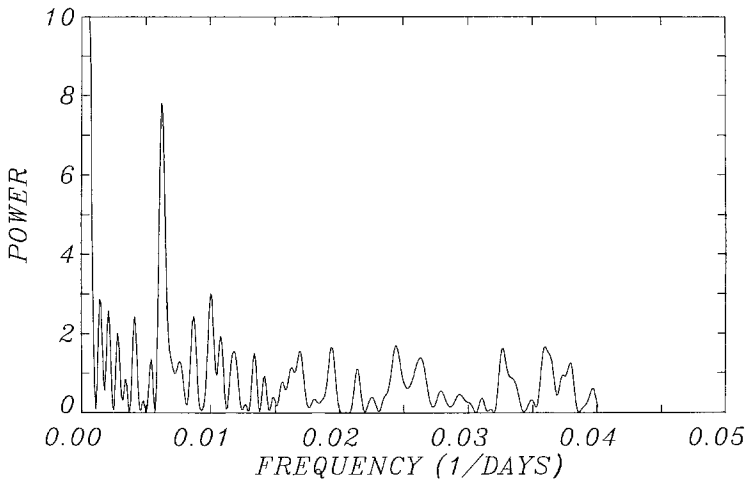


Fig. 2. Power spectrum of the rate versus time of HXRBS low energy events. Only the HXRBS events detected at energies not exceeding 150 keV were used in the analysis so that the data set would not include the gamma ray flares used by Rieger *et al.* (1985). A total of 6102 events detected from launch through July 31, 1984 were used in the analysis. The peak in the power spectrum at  $0.0633 \text{ days}^{-1}$  confirms the existence of the 158 day periodicity in this independent data set.

The interpretation of this 152–158 day periodicity in the solar flare rate during cycle 21 is still uncertain. The most complete theory has been developed by Wolff (1983) based on the rotational spectrum of *g*-modes in the Sun. He carried out a Fourier analysis of the variation of the mean monthly sunspot number in the years from 1749 to 1979 and found narrow but weak peaks in the power spectrum at a set of frequencies consistent with this model. The most prominent period found by Wolff below 200 days is 155.4 days, remarkably close to the period found for the flares in cycle 21. This period, according to Wolff's model, results from the beating between the rotation of an  $l = 2$  mode and an  $l = 3$  mode where  $l$  is the spherical harmonic index. An attempt has been made to match the beat frequencies of other  $l$ -modes to the other peaks in the power spectrum obtained from the HXRBS event rate but without success (Kiplinger, private communication).

In concluding this section, it is clear that there is compelling evidence for a periodicity in the rate of occurrence of solar flares during cycle 21 with a period on 152–158 days. It is impossible to say, at present, if this is a manifestation of the interacting *g*-modes as suggested by Wolff (1983). However, the possibility that this may be the case and the unique information concerning the solar interior that could then be determined lends great importance to this result and to the continued long-term accumulation of data.

## 2.2. THE SPECTRUM OF PEAK RATES

A second result which has been obtained from the large number of flares recorded by SMM is an accurate spectrum of peak rates involving over 6000 flares recorded with HXRBS. This differential spectrum shown in Figure 3 was obtained from all complete

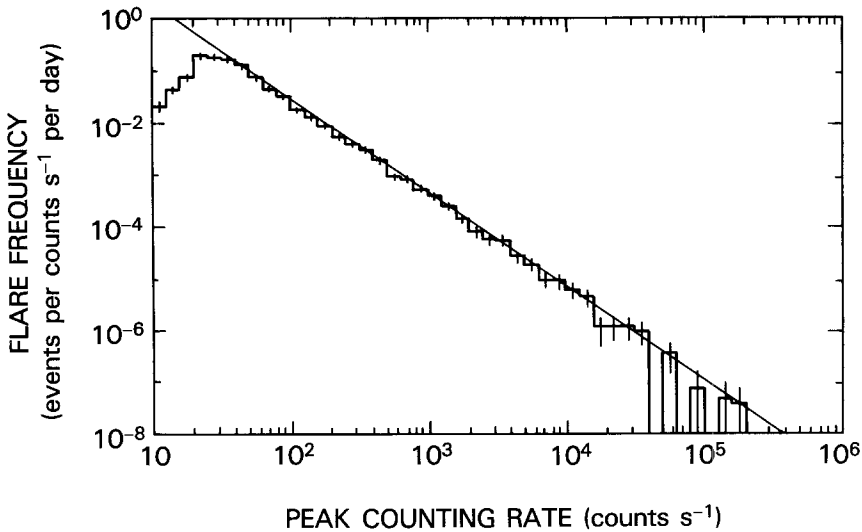


Fig. 3. Peak rate spectrum of all complete events detected with HXRBS from launch to February 1985. The straight line through the data corresponds to the power-law expression given in the text with a spectral index of  $-1.8$ .

events recorded with HXRBS above  $\sim 30$  keV between launch and the beginning of 1985 and it can be well represented by an expression of the form

$$N(P) = 110 P^{-1.8} \text{ flares (counts s}^{-1} \text{ day)}^{-1},$$

where  $N(P)$  is the rate of flares detected with a peak rate  $P$  above background measured with HXRBS as the sum of the rate in all 15 channels. This expression fits the data over more than three orders of magnitude; the turnover below a peak rate of  $\sim 40$  counts  $\text{s}^{-1}$  almost certainly results from the reduced efficiency of finding events in the HXRBS data that result in a less than doubling of the HXRBS background rate.

This differential spectrum of peak rates shown in Figure 3 is not directly comparable to the spectrum reported by Datlowe *et al.* (1974) and renormalized by Lin *et al.* (1984). Their integral spectrum is for the peak photon flux at 20 keV. It can be related to Figure 3 by noting that for a typical power-law photon spectrum with an index of 5, a peak HXRBS rate above background of 1000 counts  $\text{s}^{-1}$  corresponds to a photon flux at 20 keV of  $\sim 30$  photons  $\text{cm}^{-2} \text{s}^{-1} \text{keV}^{-1}$ . This is the highest flux included in Datlowe *et al.*'s spectrum. Thus, Figure 3 extends the spectrum some two orders of magnitude to larger events. This is possible because the effects of pulse pile-up were less severe in HXRBS than in the OSO-7 detector (Datlowe, 1975) as a result of the  $\sim 0.06$  cm thick aluminum window and the  $\sim 0.01$  cm thick dead-layer on the HXRBS CsI(Na) crystal. In spite of these relatively thick absorbers, pulse pile-up is still a problem for HXRBS when the total counting rate greatly exceeds  $10^4$  counts  $\text{s}^{-1}$ , especially when the photon spectrum is steeper than  $\sim E^{-5}$ .

There is no indication that the spectrum of peak rates changes shape as a function

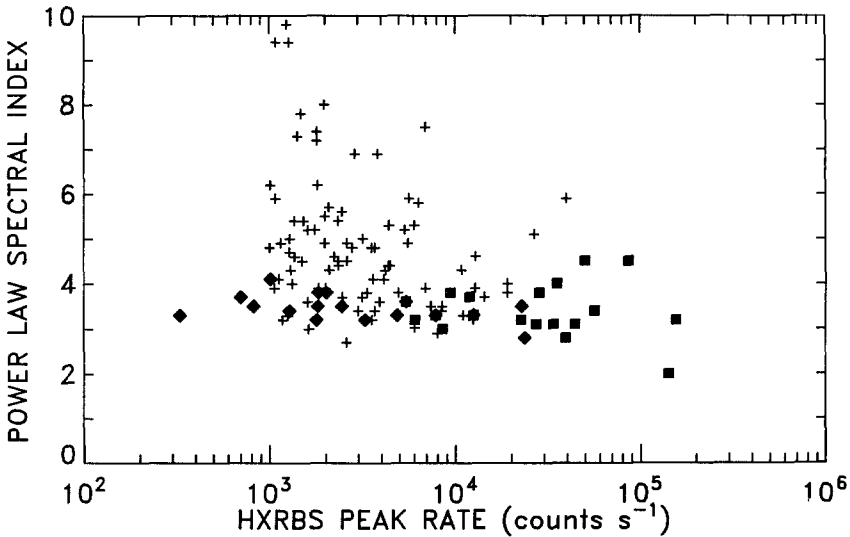


Fig. 4. The hard X-ray spectral index  $\gamma$  obtained from HXRBS data at the time of peak counting rate versus the peak counting rate summed over all 15 channels. The plus signs are for all flares in 1980 for which HXRBS recorded the true peak of the event and the peak rate was  $> 1000$  counts  $s^{-1}$ . The filled squares are for the 1980 and 1981 flares listed by Bai *et al.* (1985) that showed evidence for gamma-ray line emission in the Gamma-Ray Spectrometer (GRS) on SMM. The filled diamonds are for the gradual microwave-rich flares recorded in 1980, 1981, and 1982 and also listed by Bai *et al.* (1985).

of time. When separate spectra are obtained for each of the five years from 1980–1984, all are consistent with the same slope as that shown in Figure 4. Furthermore, the power-law slope of  $-1.8$  is consistent with the slope of  $-0.8$  obtained for the integral spectrum in 1971/1972 by Datlowe *et al.* (1974) and  $-0.9$  obtained for the integral spectrum in 1969/1971 using the detector very similar to HXRBS on OSO-5 (Dennis, unpublished).

### 2.3. DISTRIBUTION OF SPECTRAL INDEX

The HXRBS observations allow a counting rate spectrum to be obtained every 128 ms. From each such spectrum or from spectra accumulated over longer intervals, the spectrum of the incident photon flux can be determined as a function of time throughout the flares of interest. Unfortunately, as with all scintillation spectrometers such as HXRBS, the relatively poor energy resolution and the other factors contributing to the non-diagonal elements of the instrument response matrix, make it necessary to assume a form for the incident spectrum before the instrument deconvolution can be carried out. A power-law spectral form is commonly used and this can be expressed as follows:

$$N(E) = AE^{-\gamma} \text{ photons cm}^{-2} \text{ s}^{-1} \text{ keV}^{-1},$$

where  $N(E)$  is the photon flux (strictly flux density) in units of photons  $\text{cm}^{-2} \text{ s}^{-1} \text{ keV}^{-1}$  at an energy  $E$  in keV that is incident on the detector. The parameters  $A$  and  $\gamma$  are determined from the observations using the technique described by Batchelor (1984).

The power-law spectral analysis has been carried out for many HXRBS events and the results have been used to determine the spectrum and energy content of the electrons producing the bremsstrahlung X-rays (Wu *et al.*, 1985). In Figure 4 we show the distribution in the value of  $\gamma$  determined at the time of peak HXRBS counting rate for all complete flares recorded in 1980 where that peak rate was greater than 1000 counts  $\text{s}^{-1}$ . The value of  $\gamma$  is seen to range from slightly less than 3 to as high as 10. It must be realized that, again because of the poor energy resolution of scintillation spectrometers, spectra steeper than  $E^{-7}$  cannot be accurately measured, and consequently, any value of  $\gamma$  greater than  $\sim 7$  in Figure 4 should be considered as a lower limit at  $\gamma = 7$ . Corrections were applied for the effects of pulse pile-up using the technique described by Datlowe (1975, 1977) so that we believe that the variation in the mean value of  $\gamma$  with the peak rate is real. This may be a further manifestation of the Big Flare Syndrome (Kahler, 1982) such that bigger flares tend to have harder spectra. Figure 4 also shows that flares that are relatively microwave rich and those that produce gamma ray lines also have harder X-ray spectra (Bai *et al.*, 1985).

Figure 4 can be compared to the distribution of  $\gamma$  given by Datlowe *et al.* (1974) with the understanding that they were looking at smaller flares with observations extending down to lower energies: 10 keV as compared to 25 keV for HXRBS. The values of  $\gamma$  obtained by Datlowe *et al.* (1974) extend from 2 to 7 with a median value of 4.0. This is clearly at least 1.0 lower than the median value of the smallest events in Figure 4. A median value of  $\sim 5.0$  was obtained by Kane (1973) using OGO-5 data. Thus, it is possible that the generally steeper spectra found here is a result of the average spectrum being flatter from 10 to 25 keV and steeper at higher energies. This would agree with the sometimes better fit obtained at the peak of some flares to an exponential function expected for thermal bremsstrahlung (Dennis *et al.*, 1981; Kiplinger *et al.*, 1983b).

### 3. Flare Classification Schemes

It has long been known that not all flares are alike, and various classification schemes have been proposed based on the appearance of different flares in certain wavelength or energy bands and different phases. These schemes have suffered from the difficulty of relating them to one another and in determining if the different classes were merely phenomenological or actually indicated the occurrence of different physical processes. It is vitally important to determine if different processes are occurring to produce the different types of flares. It has been one of the frustrations of solar flare physics that any generalization about flares that one tries to make is immediately met with many counter examples. If the counter examples can be shown to be different types of flares with a different process producing the particle acceleration, for example, then that would be an important step forward in understanding flares.

Pallavicini *et al.* (1977) developed a useful classification scheme based on soft X-ray images of limb flares made from Skylab. They identified three principal groupings: (a) flares characterized by compact loops, (b) flares with point-like appearance, and (c) flares characterized by large and diffuse systems of loops.

Considerable advances have been made in classifying flares as a result of more recent observations. This is best exemplified by the scheme introduced by Tanaka (1983) and used by Tsuneta (1983), Ohki *et al.* (1983), and Tanaka *et al.* (1983). This scheme is based on the hard X-ray imaging results from Hinotori but has found widespread value in coordinating other observations. Tanaka (1983) also divided flares into three classes referred to as type A, B, and C, but it appears that the Pallavicini *et al.*'s A and B groups may correspond to Tanaka's type B and A flares, respectively. Some flares, particularly the larger ones, can show characteristics of more than one type during their different phases. The three different flare types have the following distinct properties:

*Type A flares:* hot thermal flares with  $T \sim 3 - 5 \times 10^7$  K, compact,  $< 5000$  km, low altitude.

*Type B Flares:* typical impulsive bursts, double footpoints seen in hard X-rays, highly sheared loop with lengths  $\gtrsim 2 \times 10^4$  km, possible existence of electron beams producing hard X-rays in thick-target interactions.

*Type C Flares:* high altitude X-ray sources,  $\sim 5 \times 10^4$  km, gradually varying X-ray and microwave fluxes, X-ray spectral hardening and microwave delay suggesting trapped non-thermal electrons and/or continuous acceleration.

In this review I shall concentrate on discussions of SMM observations of type B flares obtained mainly during 1980 and on type C flares observed mainly after 1980. I will not discuss any observations of type A flares since no good examples have been reported in the HXIS data set. The reader is referred to papers by Tsuneta *et al.* (1984a) and Tsuneta (1983) for discussion of Hinotori observations of this type of flares. There is some statistical evidence that type C flares tend to occur preferentially during the decreasing phase of the solar cycle, and this may explain the difference between the 1980 results from the SMM Hard X-Ray Imaging Spectrometer (HXIS) in 1980 and the initial 1981 results from Hinotori. It appears that primarily type B flares were detected with HXIS whereas the Hinotori team initially reported observations of type C flares.

#### 4. Properties of Type B Flares Observed with SMM

##### 4.1. THE 1980, NOVEMBER 5 FLARE AT 22:32 UT

The best example of a type B flare in the SMM data set is the flare on 1980, November 5 starting at 22:32 UT. The soft and hard X-ray time profiles are shown in Figure 5, where the earlier flare at 22:26 UT can also be seen. Although the first flare was observed at 15 GHz with the Very Large Array (Hoyng *et al.*, 1983), it was a factor of ten less intense in X-rays than the second flare and the statistical significance of the HXIS images in the highest energy bands (16–30 keV) is poor. Hence, the second flare has been the subject of more extensive study than the first flare (Duijveman *et al.*, 1982; Duijveman and Hoyng, 1983; Rust *et al.*, 1985; MacKinnon *et al.*, 1984; Wu *et al.*, 1985; Dennis *et al.*, 1985).

As shown in Figure 5, the hard X-ray time profile of this second flare was relatively

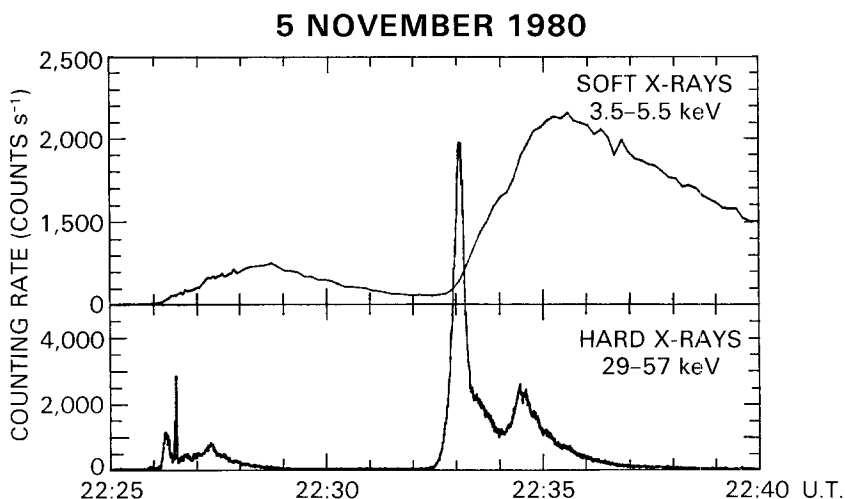


Fig. 5. Soft and hard X-ray emissions as functions of time for the two flares on 1980, November 5. The soft X-ray counting rate is the sum of the counts in the HXIS band 1 in selected pixels of the coarse field of view. The hard X-ray rate is the sum of counts in HXRBS channel 1 and 2.

simple, with a single, relatively smooth and intense spike lasting for 17 s (FWHM) followed some 90 s later by a second, less intense peak. The detailed spectral evolution of the first peak can be seen in Figure 6 where the HXRBS counting rates in three different energy ranges and the value of the power-law spectral index  $\gamma$  determined from the 34–405 keV HXRBS data are plotted on an expanded time-scale. The value of  $\gamma$  decreases from 6 near the beginning of the event to 3.5 at the time of the peak rate and increases back to  $\geq 6$  on the decay. This soft-hard-soft spectral evolution was first reported by Kane and Anderson (1970) and is considered typical for impulsive flares. Some impulsive flares, however, show high energy tails on the spectrum above 50 to 100 keV that remain hard or become harder after the peak (Crannell *et al.*, 1978; Dennis *et al.*, 1981). Indeed this is also true for the November 5 peak above  $\sim 100$  keV. It is not clear if this early indication of spectral hardening after an impulsive spike is the beginnings of a type C flare as discussed below. It is possible that there is a continuous progression from purely impulsive type B events with no spectral hardening after the peak to purely gradual type C events with continuous spectral hardening through the peak. There are some events observed with HXRBS that clearly show type B and type C characteristics on different peaks within the same flare. Hence, events classified as type B or type C may just represent the extreme cases; impulsive and gradual phases may occur in all flares at some intensity and/or energy levels. It would seem, however, that the relative importances of these two phases must differ by several orders of magnitude for flares now classified as type B and type C.

The HXIS 16–30 keV images show three well resolved bright patches during the first impulsive peak in the second flare on 1980, November 5 at 22:33 UT (Figure 7). Two patches labelled A and B following Duijveman *et al.* (1982) are separated by

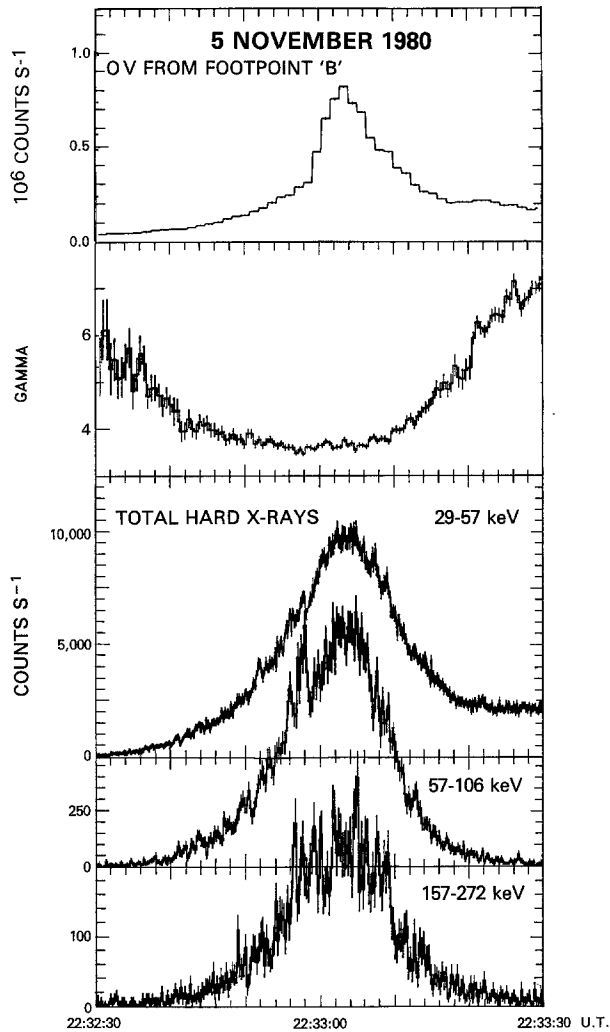


Fig. 6. An expanded plot of the major hard X-ray peak shown in Figure 5 for the 1980, November 5 flare at 22:33 UT. The bottom three graphs show the HXRBS counting rates as functions of time in three different energy ranges. The middle plot shows the variation of the power-law spectral index  $\gamma$  obtained from the 34–405 keV HXRBS counting rate data (channels 2–14) on the same time-scale. The top plot shows the time variation of the UVSP counting rate in O V summed over all 9 pixels shown in Figure 7. More than 90% of the counts came from the three southern-most pixels (Dennis *et al.*, 1985). The error bars on all the plots represent  $\pm 1\sigma$  uncertainties based on the Poisson fluctuations alone.

$1.6 \times 10^4$  km and a third patch labelled C is separated from B by  $7 \times 10^4$  km. Comparisons with  $H\alpha$  images and magnetograms suggest that the bright patches were at the footpoints of two magnetic loops joining A and B, and B and C. Duijveman *et al.* (1982) claimed that the footpoints B and C started to brighten simultaneously to within  $\sim 5$  s implying a velocity of  $\geq 2 \times 10^9$  cm s $^{-1}$  along the assumed semi-circular loop. They showed that for this velocity to be interpreted as an Alfvén velocity, the magnetic field

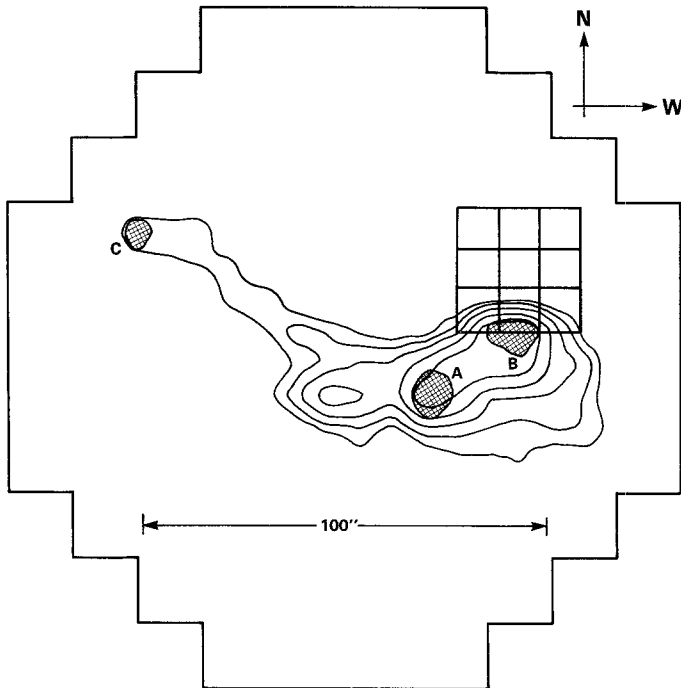


Fig. 7. Contour plot obtained from the sum of three HXIS images showing the location of the soft and hard X-ray emission at the time of the most intense hard X-ray peak on 1980, November 5. Accumulation of the first image began at 22:32:53 UT. Each image had an accumulation time of 4.5 s with a 4.5 s gap between images. The contour lines were obtained from the 3.5–8 keV data with the collimator response deconvolved according to the method given by Švestka *et al.* (1983). The contour levels are at the following counts pixel<sup>-1</sup>: 25, 50, 100, 200 and 400; the deconvolved peak rate was 902 counts pixel<sup>-1</sup>. The cross-hatched areas labelled A, B, and C were obtained from the 16–30 keV data similarly deconvolved. The outer edge of these areas corresponds to a contour level of 40 counts pixel<sup>-1</sup> for A and B and 20 counts pixel<sup>-1</sup> for C with a deconvolved peak rate at 53 counts pixel<sup>-1</sup>. The 3 × 3 array of 10" × 10" squares represents the 9 UVSP pixels used for the OV observations shown in Figure 6.

in the loop must have been  $\geq 900$  G, implausibly high for such a large loop. They concluded that the most likely explanation for the simultaneous brightening was a beam of fast electrons travelling along the loop and producing X-rays in thick-target interactions at the footpoints.

MacKinnon *et al.* (1984) have shown that only a small fraction of the hard X-rays in the HXIS 16–30 keV images come from the pixels that define the bright patches A, B, and C. They claim that the remainder come from a diffuse region around A and B although the interpretation of the two or three images at the time of the first hard X-ray burst is complicated by the presence of a diffuse background resulting from the leakage of high energy photons through the walls of the instrument collimator. This conclusion that only a small fraction of the photons come from the footpoints is supported, however, by an extrapolation of the HXRBS spectrum above 30 keV down to the 16–30 keV HXIS energy range. Good agreement is found between this extrapolated

spectrum and the total HXIS counting rate integrated over the whole fine field of view. When the counts in only the fine field of view pixels that define the three bright patches are summed, however, the resulting flux is a order of magnitude below the HXRBS extrapolation. If the spectrum of only the impulsive component is used, i.e., the more gradually varying component is subtracted from the fluxes in each energy band, then the spectrum becomes flatter at energies below 50 keV,  $E^{-3}$  compared to  $E^{-3.9}$  for the spectrum of the total flux. This reduces the discrepancy and suggests that the impulsive component comes primarily from the footpoints whereas the more gradually varying component comes from a larger area.

Rust (1984) has also suggested that the total energy in electron beams in the November 5 flare was  $\leq 10\%$  of the total energy released and that the remainder appeared as a high-temperature thermal source. Evidence from HXIS images in bands 1 and 2 for a thermal conduction front travelling to point C is given in Rust *et al.* (1985) but the interpretation of the moving contour lines is ambiguous. An equally valid interpretation would be one where the emission from loop BC increased uniformly along the loop as the plasma in the loop was heated by fast electrons travelling along the loop.

Later on in the same flare at 22 : 34 : 30 UT, a second hard X-ray peak occurred with an  $E^{-7}$  spectrum, much softer than the  $E^{-4}$  spectrum of the first peak. Furthermore, at the time of the second peak, the HXIS images show that the 16–30 keV X-rays came predominantly from a location between the original bright patches A and B. The soft X-ray flux shows a second increase at about this time, as indicated in Figure 5, suggesting that almost the same amount of energy was released as during the first impulsive peak. The simplest explanation of these observations is that this second energy release served mainly to heat the plasma injected into the loop as a result of the first non-thermal energy release. Such a transition from an essentially non-thermal model to a thermal model during the impulsive phase of many flares has been proposed by Smith (1985) and by Tsuneta (1985). Smith (1985) proposes a dissipative thermal model, a term originally suggested by Emslie and Vlahos (1980), and he suggests that an increase in the ratio of plasma to magnetic pressure (the plasma  $\beta$ ) at the energy release site later in the flare results in this transition from a non-thermal to a thermal model. It must be pointed out, however, that the blue shifts in the Ca XIX lines observed with the Bent Crystal Spectrometer (Acton *et al.*, 1980) persist into the later stages of the impulsive phase of the 1980, November 5 flare indicating continuing chromospheric evaporation with upward velocities of  $\sim 200 \text{ km s}^{-1}$  even during the second hard X-ray peak (Antonucci *et al.*, 1984).

#### 4.2. SIMULTANEOUS UV AND HARD X-RAY EMISSION

Another way to differentiate between the different flare models is to look at the timing relationship between UV and hard X-ray emission during impulsive flares. The simultaneity to within 1 s of UV and hard X-ray emission has been known since the observations of sudden ionospheric disturbances (SIDs) in conjunction with hard X-ray bursts (Donnelly and Kane, 1978; Kane *et al.*, 1979). SIDs are caused by bursts of solar UV radiation between 10 and 1030 Å coming primarily from the transition region and

low corona. The combined UVSP, HXIS, and HXRBS observations have now provided the required spatial information to allow the simultaneity of the UV and hard X-ray emissions to be used to significantly constrain the flare models.

Poland *et al.* (1982) and Cheng *et al.* (1981) have shown that the transition region line radiations – O v at 1371 Å, Si iv at 1402 Å, and O iv at 1401 Å – are strongly concentrated at the footpoints of magnetic loops. Woodgate *et al.* (1983) have shown the simultaneity of the O v emission and the 25–300 keV X-ray flux to within 1 s for several impulsive flares observed on 1980, November 8. Here we show in Figure 6 the UV and hard X-ray observations for the 1980, November 5 flare at 22:33 UT from Dennis *et al.* (1985). The total O v emission summed over all nine UVSP pixels near footpoint B shown in Figure 7 is plotted in Figure 6 on the same time-scale as the hard X-ray counting rate recorded by HXRBS in three energy ranges. This is a particularly clear example of the simultaneity to  $\lesssim 1$  s of a hard X-ray peak and the increase in the O v emission from a footpoint. It supports the conclusion reached by Woodgate *et al.* (1983) that the lack of any detectable time delay is inconsistent with flare models in which the hard X-rays are initially produced at the loop top followed by the formation of thermal conduction fronts which travel to the footpoints where the UV burst is produced by heating. Models in which both X-rays and UV radiation are both produced at the footpoints, or an electron beam transmits energy between the loop top and the footpoints in less than 1 s, are allowed by these observations.

Attempts to quantify the expected O v flux for a given electron beam intensity have met with limited success. The theoretical problem is complicated by the fact that there are two competing effects of an electron beam incident from the corona. One is the depression of the transition zone to a lower altitude and higher density. This tends to increase the amount of material at the O v emitting temperature around  $2.5 \times 10^5$  K suggesting that the O v flux should increase rapidly. The other effect suggests the opposite, however, and that is the steepening of the temperature gradient in the transition zone. This tends to reduce the amount of  $2.5 \times 10^5$  K material and suggests that the O v flux should decrease. Thus, it is important to accurately model the transition zone in any theoretical calculation of the expected O v flux and this typically is difficult to do in the computer simulations because of its extremely small scale height. Poland *et al.* (1984), Emslie and Nagai (1984), and Mariska and Poland (1985) have carried out some exploratory model calculations to study the relationship between the energy emitted in hard X-rays and in the O v line assuming that both result from an electron beam. Poland *et al.* (1984) find from the observations of individual flares that there is a definite relation between hard X-ray and O v emission throughout a given flare but that the flux ratio is different in different flares. They attribute these differences to the initial conditions in the flaring loops and their model calculations support this conclusion.

More recent observations made after the SMM repair have shown simultaneity of UV continuum and hard X-ray features in an impulsive flare to within 0.25 s (Woodgate, 1984). In a flare on 1984, May 20 at 02:59 UT, UVSP was recording at around 1600 Å with a time-resolution of 75 ms in one pixel and HXRBS was recording the counting rate above 24 keV with 10 ms time resolution. (The UVSP wavelength drive was not

working at this time so that the exact wavelength of the UV observations is not known nor is it known for certain if it was recording line or continuum emission. However, the two detectors separated by  $17 \text{ \AA}$  recorded very similar rates and consequently it is believed that they were both in the continuum with little, if any, contribution from line emission.) The overall time profile of the impulsive phase of the event in UV and hard X-rays is shown in Figure 8 and the first feature is shown on an expanded time-scale

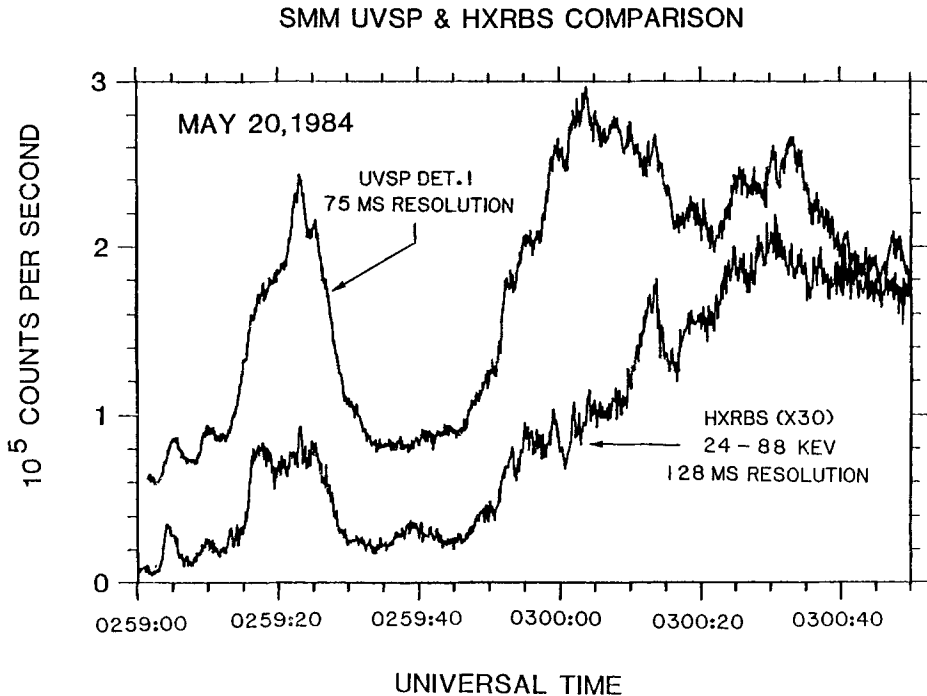


Fig. 8. Impulsive bursts during the flare on 1984, May 20 beginning at 02:59 UT showing the similarity between the hard X-ray and UV continuum time profiles.

in Figure 9. There are clearly significant differences between the overall UV and hard X-ray time profiles but the similarities are striking. In particular, the sharp feature at 02:59:23 UT shows up clearly in both time profiles with the start and peak times coincident to within 0.1 s.

If we assume that the detected UV emission for this event was continuum at  $\sim 1600 \text{ \AA}$ , then it was probably emitted low in the chromosphere at a temperature of  $\sim 5000 \text{ K}$  according to Cook and Brueckner (1979). Thus, it is difficult to see how an electron beam incident on a footpoint from the corona could result in the measured 0.1 s simultaneity since electrons cannot reach deep in the chromosphere (Woodgate, private communication). The possibility of the energy release itself occurring in the chromosphere would of course, alleviate the problem.

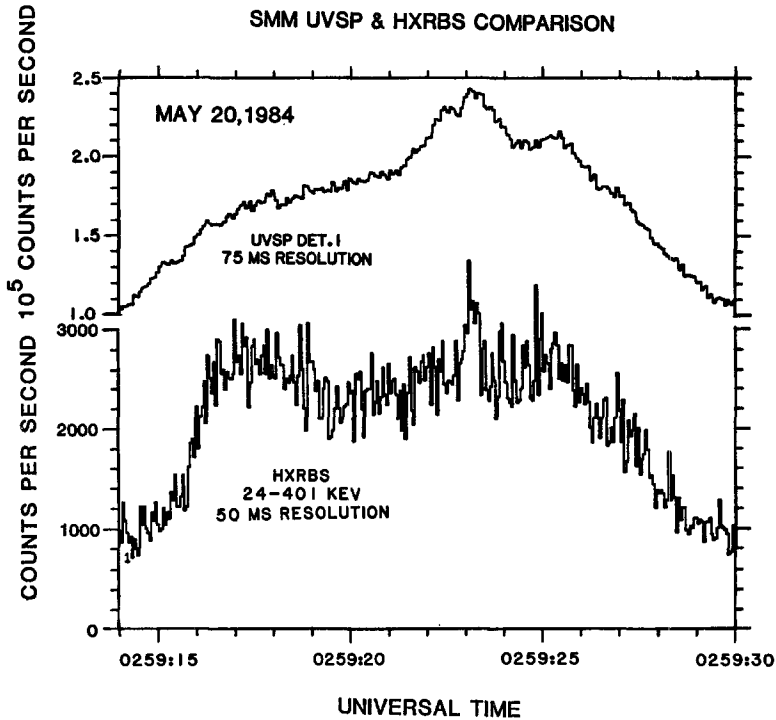


Fig. 9. The first major feature of the flare on 1984, May 20 shown in Figure 8 plotted on an expanded time-scale. The UVSP detector 1 time profile is believed to be for continuum emission at approximately  $1600 \text{ \AA}$  and has a time-resolution of 75 ms. The large scatter in the hard X-ray counting rate reflects the statistical uncertainty resulting from the mean rate at 02:59:20 UT of 115 counts per 50 ms interval. The feature at 02:59:23 UT is, however, clearly significant in both the hard X-ray and UV time profiles.

Even more recent coincident UV and hard X-ray observations with 128 ms time resolution should ultimately help to differentiate between the different possible models. An impulsive flare on 1985, April 24 at 01:48 UT was recorded by both UVSP and HXRBS. UVSP was recording separately the emission in both of the O v line and the continuum  $17 \text{ \AA}$  from the line with a time-resolution of 128 ms. Thus, the time profiles of the emission from the transition zone and from the lower chromosphere were obtained at the same time as the hard X-ray profile above 25 keV. The three time profiles are shown on the same time-scale in Figure 10, where the rich detail is evident in this flare. It is too early in the analysis of this data to make any definitive statement about the relative timing, but it does appear as if the first peak in hard X-rays and in the continuum emission are coincident to within 1 s. The O v emission, however, seems to reach its first peak a second or so later. This surprising result, if it can be verified, would support the idea that at least the initial energy release occurs in the chromosphere and not in the corona.

## SMM UVSP &amp; HXRBS COMPARISON

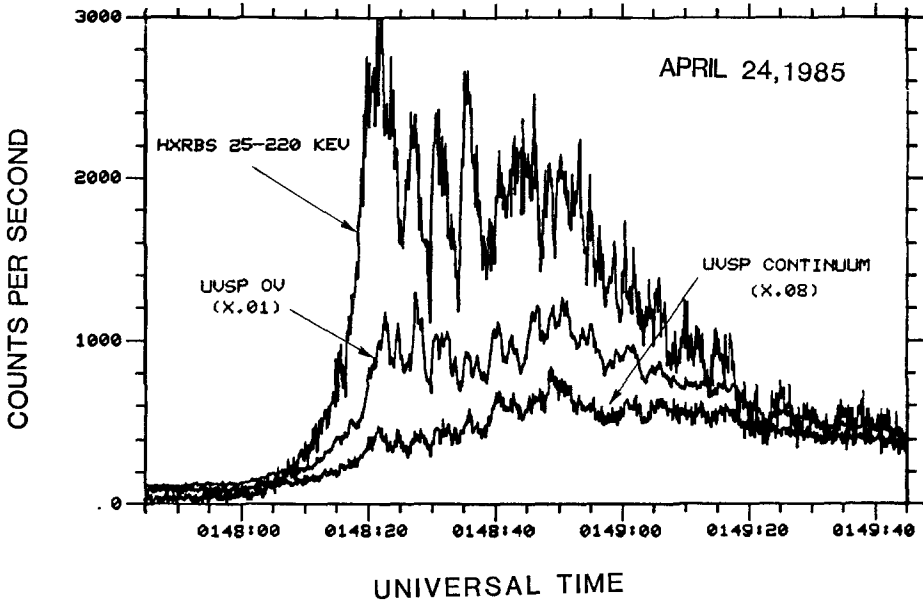


Fig. 10. UVSP and HXRBS time profiles for the flare on 1985, April 24 at 01:48 UT. The top profile is the hard X-ray counting rate between 25 and 220 keV, the center profile is the counting rate in the O VI line, and the bottom profile is the counting rate in the continuum 17 Å from the O VI line. The time-resolution for all three profiles is 128 ms,

#### 4.3 RAPID FLUCTUATIONS IN THE HARD X-RAY FLUX

The impulsive phase of solar flares is characterized by rapid variations in the hard X-ray and microwave flux. This must reflect the variations in the rate of energy release in the flare and the production of energetic electrons but the propagation of the electrons from the site of energy release to the location is also a factor in determining the observed variations. A detailed analysis of the most rapid variations that are observed has proved to be a useful tool to place limits on the models for the production and propagation of fast electrons.

Before 1980, observations of hard X-rays had revealed variations on time-scales as short as 1 s but as soon as better time-resolutions become available, variations on time-scales as short as a few tens of ms were observed (Orwig *et al.*, 1981; Kiplinger *et al.*, 1983a; Hurley *et al.*, 1983).

One of the fastest variations observed with HXRBS is shown in Figure 11, where two seconds of the counting rate are plotted with a time-resolution of 20 ms for an impulsive event that occurred on 1980, June 6. The most dramatic variation is the large, unresolved rise from 20 to 53 counts per 20 ms at 23:34:45.7 UT. Numerous other fast variations (not shown) occurring within 10s of the plotted interval support the reality of this rapid fluctuation.

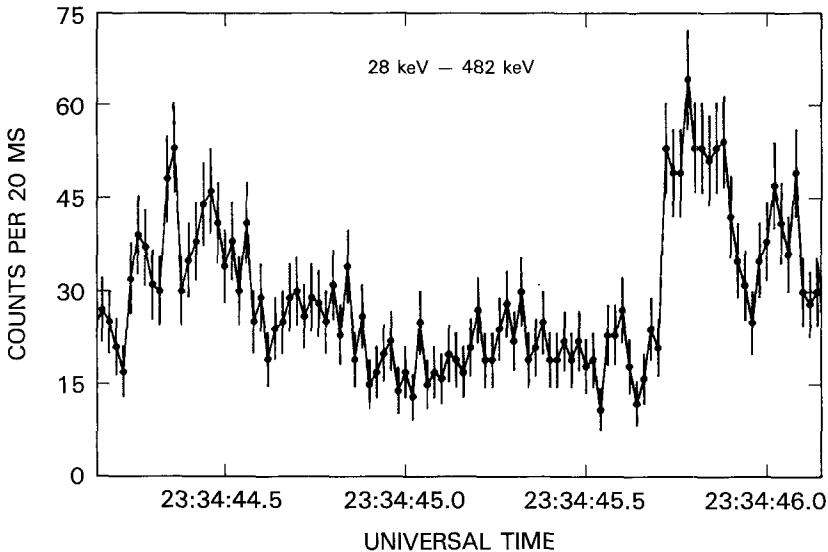


Fig. 11. Two seconds of HXRBS memory data showing very rapid X-ray variations in a solar flare which occurred on 1980, June 6. The counting rate is plotted at a time resolution of 20 ms per point with  $\pm 1\sigma$  statistical error bars.

It must be remembered that only about 10% of all flares detected with HXRBS with a sufficiently high counting rate to see variations on a sub-second time-scale, in fact, showed such rapid variations (Kiplinger *et al.*, 1983a). Thus, sub-second variations are not a common phenomenon. Nevertheless, they can be used to constrain models for energy release and propagation. The short time-scales involved are upper limits to the time-scales of the acceleration process itself. Although both thermal and non-thermal interpretations of sub-second variations are viable, Kiplinger *et al.* (1983a) have shown that a thermal interpretation has no energetic advantage over a non-thermal interpretation for the production of the hard X-rays. Furthermore, Kiplinger *et al.* (1984) have shown for a particularly well resolved sub-second spike, that the observations allow constraints to be placed on the loop length and on the electron pitch-angle distribution assuming a non-thermal interpretation.

### 5. Properties of Type C Flares

The canonical type C flare identified in the Hinotori data is the flare on 1981, May 13 (Tsuneta *et al.*, 1984b). A part of the time profile of this event as determined with HXRBS is shown in Figure 12 together with the evolution of the power-law spectral index  $\gamma$ . We see immediately two differences between this event and the 1980, November 5 event shown in Figures 5 and 6. First of all, the 1981, May 13 flare is a much more gradually varying event with the hard X-ray peak lasting for  $\sim 8$  min (FWHM) compared to 17 s for the major peak on November 5. The beginning of the event was not seen with HXRBS since SMM did not emerge from spacecraft night until

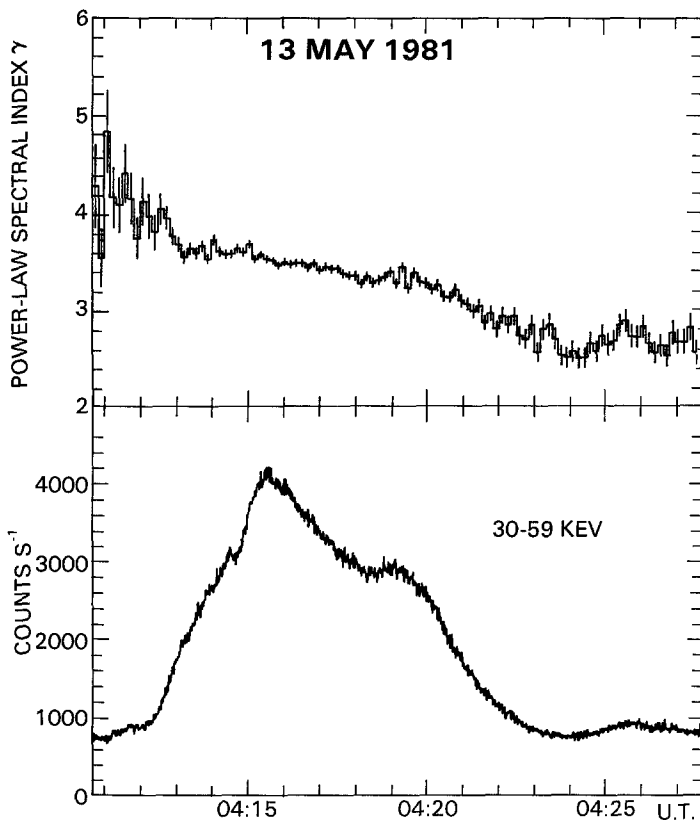


Fig. 12. The bottom trace shows the variation of the HXRBS 30–59 keV (channels 1 and 2) counting rate vs time for the major peak of the 1980, May 13 event. The upper trace shows the value of the best fit power-law spectral index  $\gamma$  as a function of time. The spectral fits were made using the HXRBS counting rates in channels 3–14 (59–419 keV) to show the spectral hardening through the peak and on the decay. Individual spectra at different times during the event are shown in Figure 13.

04:08 UT but Tsuneta *et al.* (1984b) report that this event showed no impulsive component in either hard X-rays or microwaves. The second difference is that for the May 13 event the hard X-ray spectrum gets progressively harder ( $\gamma$  decreases) through the peak in contrast to the soft-hard-soft spectral evolution of the November 5 event shown in Figure 6. The soft-hard-harder spectral evolution is also evident in Figure 13 where individual spectra are plotted for specific times on the rise and decay of the hard X-ray peak. The photon flux density was determined as a function of photon energy from the 15-channel HXRBS counting rate data using the technique described by Batchelor (1984) and a power-law fit was made to the points corresponding to channels 3–14. The lower two channels were excluded because there is a steep, low-energy component to the spectrum near the beginning of the rise and towards the end of the decay of the event as shown in Figure 13. Clearly, it is the spectrum above  $\sim 60$  keV that participates in the spectral hardening with time. The steep spectrum at lower

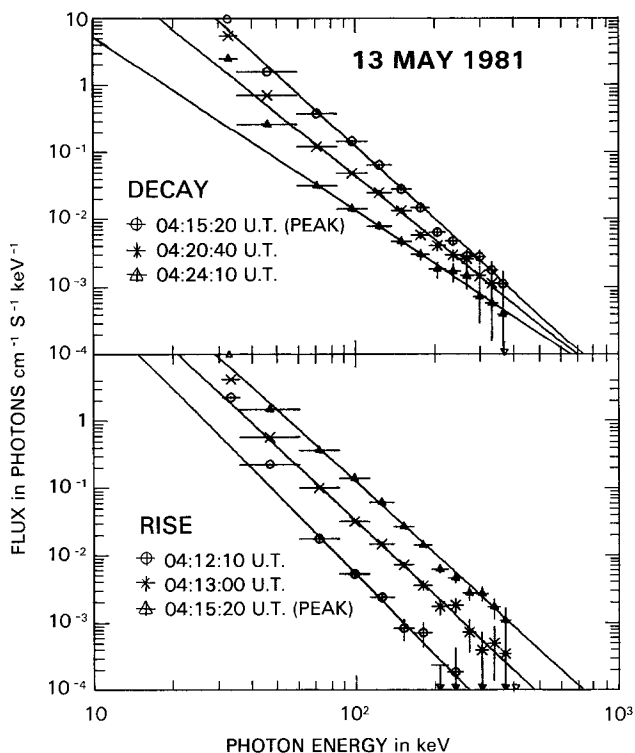


Fig. 13. Hard X-ray spectra at five different times during the major feature of the 1981, May 13 event shown in Figure 12. The data points were derived from the HXRBS counting rates assuming the indicated least-squares power-law fit through the points for channels 3–14. The vertical lines through the data points are  $\pm 1\sigma$  error bars based on the statistical uncertainties alone. The horizontal lines through the points are not error bars but indicate the widths of the HXRBS channels.

energies is most probably a high temperature thermal component similar to that reported by Lin *et al.* (1981).

The most striking result concerning the May 13 flare, however, is that the altitude of the X-ray and microwave source was  $\sim 4 \times 10^4$  km above the photosphere (Tsuneta *et al.*, 1984b). This result was obtained from the 14–38 keV image in Figure 14, which shows that the X-ray source was displaced by  $\sim 1$  arc min towards the limb from the two-ribbon  $H\alpha$  flare. Considering the location of the  $H\alpha$  source at N 9–13 E, 54–48 (*Solar Geophysical Data*), this displacement corresponds to the altitude indicated above. This is again in marked contrast to the type B flares, where at least a large fraction of the hard X-rays are believed to come from low altitudes at the footpoints of magnetic loops.

Since hard X-ray imaging has not been available for many flares, attempts have been made to select type C flares based on their more readily available properties. Cliver *et al.* (1985) have selected ten gradual hard X-ray bursts (GHB's) including the 1981, May 13 event that all show the following similar characteristics:

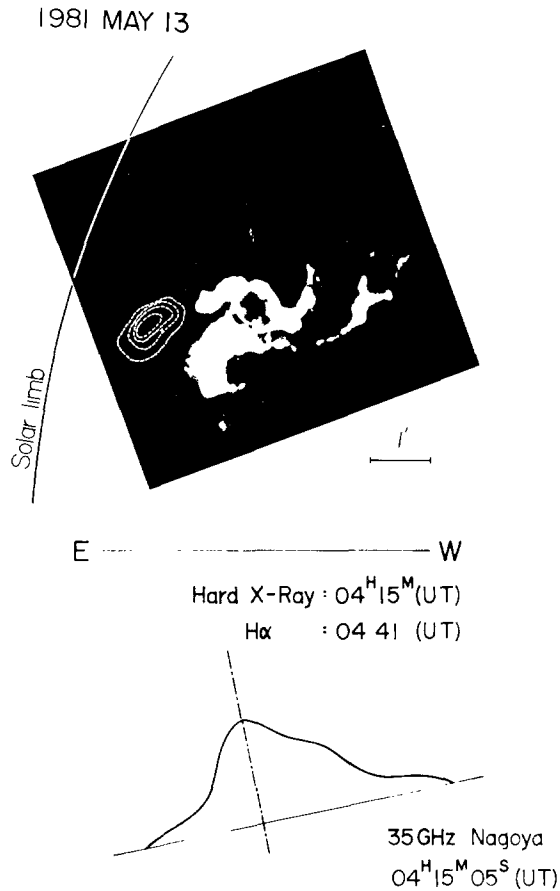


Fig. 14. Overlay from Tsuneta (1983) of the Hinotori hard X-ray image of the 1981, May 13 type C flare with an H $\alpha$  photograph taken 26 min later. The one-dimensional microwave brightness distribution at 35 GHz is oriented to show that the bulk of this emission was from the same high altitude location as the X-ray source (Kawabata *et al.*, 1983).

- (1) the X-ray spectrum is harder than average (see Figure 4) with a typical value for  $\gamma$  of between 3 and 4;
- (2) the hard X-ray spectrum systematically hardens (or at least does not soften) through the peaks and on the decay;
- (3) the GHB's are often preceded, by as much as 60 min, by an impulsive phase although sometimes, as in the case of the 1981, May 13 event, no impulsive phase may be seen at all;
- (4) the GHB's occur in the later, parallel-ribbon phase of major flares;
- (5) a coronal mass ejection was observed, or inferred, in association with at least nine of the ten GHB's;
- (6) the associated microwave bursts were also very gradual and peaked sometimes many minutes after the hard X-ray peak as shown for the 1981, April 26 flare in Figure 15;

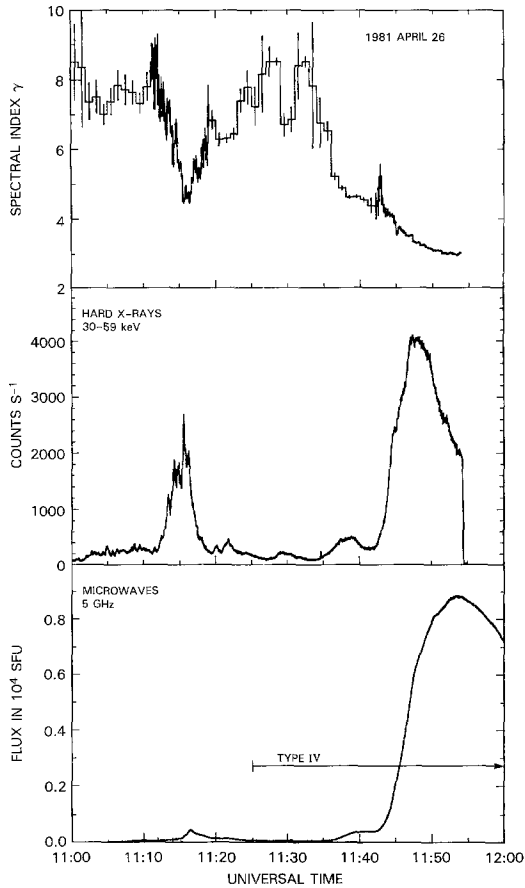


Fig. 15. Hard X-ray and microwave time-intensity profiles of the 1981, April 26 solar flare. The upper panel shows the variation of the X-ray power-law spectral index  $\gamma$  with time.

(7) the GHB's were typically microwave rich in comparison with the hard X-ray flux as shown in Figure 16 and had relatively low peak frequencies suggesting a low density source and weak magnetic fields;

(8) the GHB's are associated with long duration soft X-ray events suggesting continuous energy release for up to several hours.

These properties of GHB's lead Cliver *et al.* (1985) to propose that these events result from particle acceleration by magnetic reconnection following a coronal mass ejection. This simplified picture of such an event shown in Figure 17 was first proposed by Cliver (1983). In this model, the magnetic field lines are envisioned as being stretched as the coronal mass ejection moves out. Magnetic reconnection takes place below the ejected material and it is at this point that the electrons are accelerated. Electrons moving upwards produce the associated radio type IV emission; electrons moving downwards are trapped in the low density loops below the reconnection point and produce the hard X-rays and microwaves.

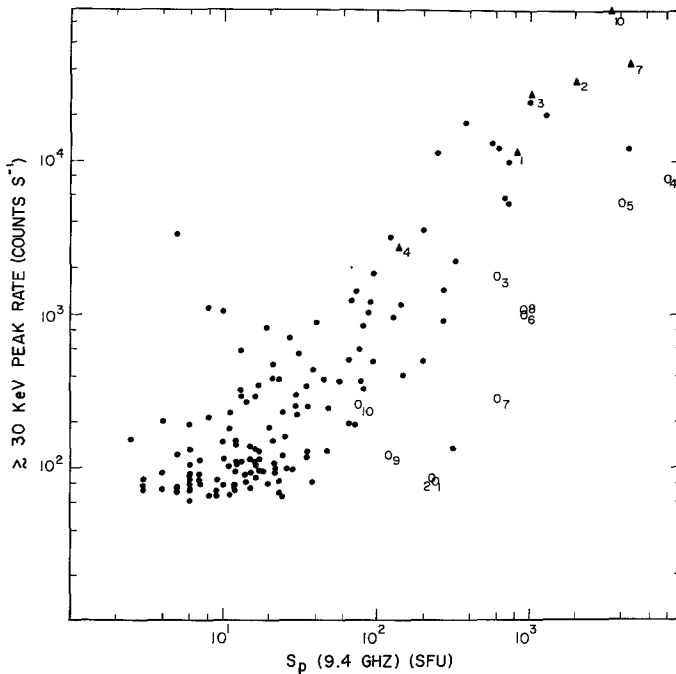


Fig. 16. Scatter plot of HXRBS  $> 30$  keV peak hard X-ray count-rate vs the peak 9.4 GHz flux-density for impulsive ( $\Delta$ ) and gradual ( $\circ$ ) components of the GHBs analysed by Cliver *et al.* (1985). For comparison, the data points for  $\sim 130$  impulsive events observed both by SMM and Toyokawa Observatory during April, August, and December 1981 are also plotted ( $\bullet$ ). For the comparison sample, we considered events to be impulsive if the 9.4 GHz emission peak occurred within  $\pm 0.5$  min of the HXRBS  $> 30$  keV maximum. The  $\sim 40$  counts  $s^{-1}$  HXRBS background counting rate was not subtracted from the  $> 30$  keV peak rates.

It is not certain if the observed spectral hardening can be attributed to the decrease in energy loss rate with increasing electron energy in the trap or to the time dependence of the electron acceleration process itself. The density of the X-ray emitting source for the 1981, May 13 flare has been estimated by Tsuneta *et al.* (1984b) to be  $3 \times 10^{10} \text{ cm}^3$  from the soft X-ray observations. The decay time for 100 keV electrons in a trap with this density would be  $\sim 1$  s assuming only Coulomb losses. Bai and Dennis (1985) give this argument and others in favor of the so-called second-step acceleration interpretation (Bai and Ramaty, 1979), in which protons are accelerated to  $> 1$  MeV and electrons to relativistic energies using particles accelerated by the primary (or first step) mechanism as injection particles. For other flares where density information is not generally available, a combination of both continuous acceleration and energy losses may well be important.

## 6. Conclusions

We have reviewed some of the more important results from SMM that have contributed greatly to our understanding of the processes that lead to the high-energy X-ray aspects

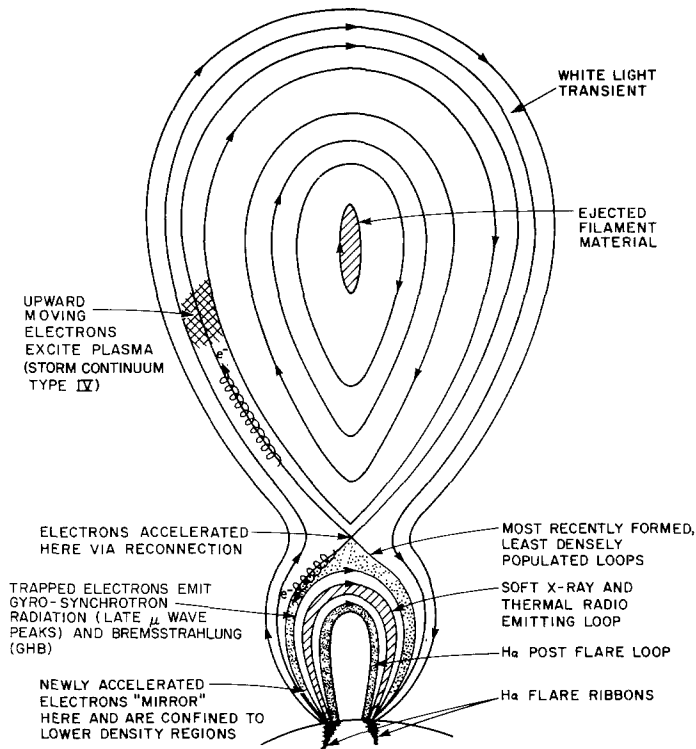


Fig. 17. Proposed geometry in which electrons accelerated via neutral 'point' reconnection are trapped and give rise to gradual hard X-ray bursts and secondary microwave peaks. The figure also indicates how concomitant type IV storm continuum might occur. The drawing is not to scale. Characteristic heights of the soft X-ray loops and the leading edge of the transient at a time  $\sim 30$  min after the flare flash phase are  $\sim 3 \times 10^4$  km, respectively.

of solar flares. The 152–158 day periodicity in the rate of occurrence of hard X-ray flares and other manifestations of solar activity may prove to be important in determining the dynamics of solar rotation as Wolff (1983) believes but only further analysis and more extensive data sets will resolve that issue. The classification of flares into three different types suggests that we are beginning to be able to distinguish between the three basic models for X-ray production: the purely thermal emission from type A flares, the thick-target interactions at the footpoints in the impulsive type B flares, and the coronal thin-target interactions in the gradual type C flares. This interpretation is still controversial and many flares exhibit characteristics of all three types. Nevertheless, the fact that in certain flares we have begun to distinguish between the different models for X-ray production has allowed us to refine the constraints on the basic flare energy release mechanism or mechanisms.

Higher-resolution hard X-ray images with better time resolution and extending to higher photon energies will allow us to improve the identification of the correct X-ray production models in any specific flare. The simultaneity of footpoint brightening on

time scales of fractions of a second is a very powerful indicator of the existence of electron beams. The detection of the thin-target emission from such beams in the loop would also give a clear picture of where the particles are accelerated in the loop and with what pitch-angle distributions. Imaging to energies above the 30–40 keV achieved with SMM and Hinotori is necessary to clearly separate the thermal emission of the  $10\text{--}30 \times 10^6$  K plasma from the higher energy X-ray component. Furthermore, higher spectral resolution than is possible with scintillation spectrometers is required to clearly resolve the very steep spectra of this thermal emission.

These requirements for future observations are well within the capabilities of new instruments being proposed for flights during the next solar maximum. Thus, the opportunity exists to build on our successes during this cycle 21 of solar activity and to achieve even more dramatic advances in our understanding of the fundamental flare processes during cycle 22.

### Acknowledgements

I am grateful to Larry Orwig, Alan Kiplinger, and the HXRBS and SMM computer staff for their assistance in data analysis. I have benefitted greatly from the freely shared ideas of many people and the open access to the SMM and ground-based observations from many groups around the world. In particular, I wish to acknowledge the use of UVSP data thanks to Bruce Woodgate, the SOON microwave observations thanks to Ed Cliver, and the Hinotori,  $H\alpha$ , and microwave results shown in Figure 14 thanks to S. Tsuneta. Finally, I much appreciate the careful reading of an early manuscript by Alan Kiplinger and Takeo Kosugi, and the rapid typing of Gloria Wharen.

### References

- Acton, L. W., Culhane, J. L., Gabriel, A. H., and 21 co-authors: 1980, *Solar Phys.* **65**, 53.  
 Antonucci, E., Gabriel, A. H., and Dennis, B. R.: 1984, *Astrophys. J.* **287**, 179.  
 Bai, T.: 1982, in R. E. Lingenfelter, H. S. Hudson, and D. M. Worrall (eds.), *Gamma Ray Transients and Related Astrophysical Phenomena*, American Institute of Physics, New York, p. 409.  
 Bai, T. and Dennis, B. R.: 1985, *Astrophys. J.* **292**, 699.  
 Bai, T. and Ramaty, R.: 1979, *Astrophys. J.* **227**, 1072.  
 Bai, T., Hudson, H. S., Pelling, R. M., Lin, R. P., Schwartz, R. A., and von Rosenvinge, T. T.: 1983, *Astrophys. J.* **267**, 433.  
 Bai, T., Kiplinger, A. L., and Dennis, B. R.: 1985, *Astrophys. J.* (in preparation).  
 Batchelor, D. A.: 1984, Ph.D. Thesis, University of North Carolina at Chapel Hill; also NASA TM86102.  
 Bogert, R. S. and Bai, T.: 1985, presented at the Solar Physics Division meeting Tucson, May 13–15, 1985.  
 Brown, J. C.: 1971, *Solar Phys.* **18**, 489.  
 Cheng, C.-C., Tandberg-Hanssen, E., Bruner, E. C., Orwig, L. E., Frost, K. J., Woodgate, B. E., and Shine, R. A.: 1981, *Astrophys. J.* **248**, L39.  
 Cliver, E. W.: 1983, *Solar Phys.* **84**, 347.  
 Cliver, E. W., Dennis, B. R., Kane, S. R., Neidig, D. F., Sheeley, N. R., Jr., and Koomen, M. J.: 1985, *Astrophys. J.* (submitted).  
 Cook, J. W. and Brueckner, G. E.: 1979, *Astrophys. J.* **227**, 645.  
 Crannell, C. J., Frost, K. J., Mätzler, C., Ohki, K., and Saba, J. L.: 1978, *Astrophys. J.* **223**, 620.  
 Datlowe, D. W.: 1975, *Space Sci. Instr.* **1**, 389.  
 Datlowe, D. W.: 1977, *Nucl. Inst. Methods* **145**, 365.

- Datlowe, D. W., Elcan M. J., and Hudson, H. S.: 1974, *Solar Phys.* **39**, 155.
- Deeming, T. J.: 1975, *Astrophys. Space Sci.* **36**, 137.
- Dennis, B. R., Frost, K. J., and Orwig, L. E.: 1981, *Astrophys. J.* **244**, L167.
- Dennis, B. R., Frost, K. J., Orwig, L. E., Kiplinger, A. L., Dennis, H. E., Gibson, B. R., Kennard, G. S., and Tolbert, A. K.: 1983, NASA TM84998.
- Dennis, B. R., Kiplinger, A. L., Orwig, L. E., and Frost, K. J.: 1985, *Proc. 2nd India-U.S. Workshop on Solar Terrestrial Physics, January 1984*, New Delhi, India; also NASA TM86187.
- Donnelly, R. F. and Kane, S. R.: 1978, *Astrophys. J.* **222**, 1043.
- Duijveman, A. and Hoyng, P.: 1983, *Solar Phys.* **86**, 289.
- Duijveman, A., Hoyng, P., and Machado, M. E.: 1982, *Solar Phys.* **81**, 137.
- Emslie, A. G. and Nagai, F.: 1984, *Astrophys. J.* **279**, 896.
- Emslie, A. G. and Vlahos, L.: 1980, *Astrophys. J.* **242**, 359.
- Hoyng, P., Marsh, K. A., Zirin, H., and Dennis, B. R.: 1983, *Astrophys. J.* **268**, 865.
- Hurley, K., Niel, M., Talon, R., Estulin, I. V., and Dolidge, V. Ch.: 1983, *Solar Phys.* **86**, 367.
- Kahler, S. W.: 1982, *J. Geophys. Res.* **87**, 3439.
- Kane, S. R.: 1973, in R. Ramaty and R. G. Stone (eds.), *High Energy Phenomena in the Sun*, NASA SP-342, p. 55.
- Kane, S. R. and Anderson, K. A.: 1970, *Astrophys. J.* **162**, 1003.
- Kane, S. R., Frost, K. J., and Donnelly, R. F.: 1979, *Astrophys. J.* **234**, 669.
- Kawabata, K., Ogawa, H., and Suzuki, I.: 1983, *Solar Phys.* **86**, 247.
- Kiplinger, A. L., Dennis, B. R., Emslie, A. G., Frost, K. J., and Orwig, L. E.: 1983a, *Astrophys. J.* **265**, L99.
- Kiplinger, A. L., Dennis, B. R., Frost, K. J., and Orwig, L. E.: 1983b, *Astrophys. J.* **273**, 783.
- Kiplinger, A. L., Dennis, B. R., Frost, K. J., and Orwig, L. E.: 1984, *Astrophys. J.* **287**, L105.
- Kiplinger, A. L., Dennis, B. R., and Orwig, L. E.: 1985, *Bull. Am. Astron. Soc.* **16**, 891.
- Leach, J. and Petrosian, V.: 1983, *Astrophys. J.* **269**, 715.
- Lin, R. P. and Hudson, H. S.: 1976, *Solar Phys.* **50**, 153.
- Lin, R. P., Schwartz, R. A., Kane, S. R., Pelling, R. M., and Hurley, K. C.: 1984, *Astrophys. J.* **283**, 421.
- Lin, R. P., Schwartz, R. A., Pelling, R. M., and Hurley, K. C.: 1981, *Astrophys. J.* **251**, L109.
- MacKinnon, A. L., Brown, J. C., and Hayward, J.: 1984, preprint.
- Mariska, J. T. and Poland, A. I.: 1985, *Solar Phys.* **96**, 317.
- Ohki, K., Takakura, T., Tsuneta, S., and Nitta, N.: 1983, *Solar Phys.* **86**, 301.
- Orwig, L. E., Frost, K. J., and Dennis, B. R.: 1981, *Astrophys. J.* **244**, L163.
- Pallavicini, R., Serio, S., and Vaiana, G. S.: 1977, *Astrophys. J.* **216**, 108.
- Poland, A. I., Machado, M. E., Wolfson, C. J., Frost, K. J., Woodgate, B. E., Shine, R. A., Kenny, P. J., Cheng, C.-C., Tandberg-Hanssen, E. A., Bruner, E. C., and Henze, W.: 1982, *Solar Phys.* **78**, 201.
- Poland, A. I., Orwig, L. E., Mariska, J. T., Nakatsuka, R., and Auer, L. H.: 1985, *Astrophys. J.* **280**, 457.
- Pryor, H., Pierce, M. J., Speich, D. M., Fesq, L. M., Spear, K. A., Nelson, J. J., and McGovern, J. G.: 1981, Solar Maximum Mission Event Listing, Internal Document of the SMM Data Analysis Center, NASA, GSFC.
- Rieger, E., Share, G. H., Forrest, D. J., Kanback, G., Reppin, C., and Chupp, E. L.: 1985, *Nature* **312**, 623.
- Rust, D. M.: 1984, *Adv. Space Res.* **4**, 191.
- Rust, D. M., Simnett, G. M., and Smith, D. F.: 1985, *Astrophys. J.* **288**, 401.
- Smith, D. F.: 1985, *Astrophys. J.* **288**, 801.
- Švestka, Z., Schrijver, J., Somov, B., Dennis, B. R., Woodgate, B. E., Fürst, E., Hirth, W., Klein, L., and Raoult, A.: 1983, *Solar Phys.* **85**, 313.
- Tanaka, K., 1983, in P. B. Byrne and M. Rodono (eds.), 'Activity in Red-Dwarf Stars', *IAU Colloq.* **71**, 307.
- Tanaka, K., Nitta, N., Akita, K., and Watanabe, T.: 1983, *Solar Phys.* **86**, 91.
- Tramiel, L. J., Charan, G. A., and Novick, R.: 1984, *Astrophys. J.* **280**, 440.
- Tsuneta, S.: 1983, in J.-C. Pecker and Y. Uchida (eds.), *Proc. Japan-France Seminar on Active Phenomena in the Outer Atmosphere of the Sun and Stars, 3-7 October 1983*, CNRS and Observatoire de Paris, p. 243.
- Tsuneta, S.: 1985, *Astrophys. J.* **290**, 353.
- Tsuneta, S., Nitta, N., Ohki, K., Takakura, T., Tanaka, K., Makishima, K., Murakami, T., Oda, M., and Ogawara, Y.: 1984a, *Astrophys. J.* **284**, 827.
- Tsuneta, S., Takakura, T., Nitta, N., Ohki, K., Tanaka, K., Makishima, K., Murakami, T., Oda, M., Ogawara, Y., and Kondo, I.: 1984b, *Astrophys. J.* **280**, 887.
- Tucker, W. H.: 1975, *Radiation Processes in Astrophysics*, MIT Press, Cambridge.

Wolff, C. L.: 1983, *Astrophys. J.* **264**, 667.

Woodgate, B. E.: 1984, *Adv. Space Res.* **4**, 393.

Woodgate, B. E., Shine, R. A., Poland, A. I., and Orwig, L. E.: 1983, *Astrophys. J.* **265**, 530.

Wu, S. T., de Jager, C., Dennis, B. R., Hudson, H. S., Simnett, G. M., Strong, K. T., Bentley, R. D., Bornmann, P. L., Bruner, M. E., Cargill, P. J., Crannell, C. J., Doyle, J. G., Hyder, C. L., Kopp, R. A., Lemen, J. R., Martin, S. F., Pallavicini, R., Peres, G., Serio, S., Sylvester, J., and Veck, N. J.: 1985, in M. R. Kundu and B. E. Woodgate (eds.), *Proc. SMM Workshop on Solar Flares*, NASA, (in preparation).